PCCP

Accepted Manuscript

ROYAL SOCIETY OF CHEMISTRY

www.rsc.org/pccp

Physical Chemistry Chemical Physics RSCPublishing

ARTICLE

Extinction Measurements for Optical Band Gap Determination of Soot in a Series of Nitrogen-Diluted Ethylene/Air Non-Premixed Flames

Erin M. Adkins [a] and J. Houston Miller [a]

Cite this: DOI: 10.1039/x0xx00000x

Received 00th January 2012,
Accepted 00th January 2012

DOI: 10.1039/x0xx00000x

www.rsc.org/

Visible light extinction was measured in a series of nitrogen-diluted, ethylene/air, non-premixed flames and this data was used to determine the optical band gap, OBG, as a function of flame position. Collimated light from a supercontinuum source is telescopically expanded and refocused to match the *f*–number of a dispersing monochromator. The dispersed light is split into a power metering channel and a channel that is periscoped and focused into the flame. The transmitted light is then recollimated and focussed onto a silicon photodiode detector. After tomographic reconstruction of the radial extinction field, the OBG was derived from the near-edge absorption feature using Tauc/Davis-Mott analysis. A slight evolution in OBG was observed throughout all flame systems with a consistent range of OBG observed between approximately 1.85 eV and 2.35 eV. Averaging over all positions the mean OBG was approximately 2.09 eV for all flame systems. Comparing these results to previously published computational results relating calculated HOMO-LUMO gaps for a variety of D_{2h} PAH molecules to the number of aromatic rings in the structure, showed that the observed optical band gap is consistent with a PAH of about 14 rings or a conjugation length of 0.97 nm. This work provides experimental support to the model of soot formation where the transition from chemical to physical growth starts at a modest molecular size; about the size of circumpyrene.

Introduction

Despite increasing emphasis on alternative energy sources, 82% of the energy consumed in the United States annually is produced through combustion processes.[1] This number is only projected to decline to 80% by 2040.[1] Black Carbon (BC) or soot is a by-product of combustion produced under fuel-rich conditions when incomplete combustion results in a portion of the fuel carbon to be converted into fine particulate matter.[2] Because combustion will continue to dominate the energy sector for decades to come, the potential for significant environmental and health consequences from soot emissions will also remain a challenge.

Estimating soot's impact on climate is complicated because it not only scatters and absorbs radiation in the atmosphere, but also acts indirectly on the earths radiative energy balance by reducing the albedo of snow and glacier surfaces and it plays a role in cloud formation.[2] Characterizing these convoluted radiative effects and understanding black carbon's complex temporal and spatial global distribution makes it extremely difficult to quantify the net climate impact of soot.[2, 3] However, estimates for radiative forcing as high as 1.1 W/m^2 have been made, suggesting that soot is the second most important anthropogenic emission in terms of its climate forcing falling between CO_2 (1.85 W/m^2) and CH_4 (0.51 W/m^2).[4] The fact that soot's atmospheric lifetime (measured in days) is short compared to these other greenhouse gases (with lifetimes of decades) suggests that emphasizing soot mitigation strategies will delay or slow climate change over the coming decades giving greenhouse gas mitigation strategies a chance to take hold.

In addition to soot's role in climate change, it also has a large impact on environmental health. Within the United States, Black Carbon is estimated to account for approximately 12% of all direct ambient fine particle emissions, particles below 2.5 μm.[5] These small sized particles are thought to be responsible for a range of cardiovascular and respiratory effects. There have been studies that suggest that soot may act as a carrier for toxic combustion by-products, which introduces additional health effects.[5] Thus, reducing emission of soot into the environment will provide both short and long-term environmental benefits. To that end, development of a fundamental understanding of the chemical and physical processes in combustion systems that lead to soot will be necessary.

Experimental and computational studies over the last several decades have greatly improved our understanding of particulate formation processes in flames. It is generally agreed that the process begins with cyclization reactions of unsaturated hydrocarbon radicals to form benzene.[6-14] Subsequent growth occurs through hydrogen abstraction followed by successive acetylene addition (known as the HACA mechanism)[8] leading to larger, pericondensed aromatic hydrocarbons. (In some flame systems, recent data suggests that a comparable reaction sequence known as hydrogen abstraction methyl addition might occur).[15] It has long been thought that these polyaromatic hydrocarbons (PAH) play an important role in continued growth that leads to particle inception.[16] Once primary particles are formed, these nascent soot particles undergo surface growth (and in some systems competing oxidation reactions), and the small particles will agglomerate into larger fractal structures.[12, 17]

This theoretical framework is largely based on experimental evidence from either the beginning (concentration measurements of small, gas phase, molecular species) or the end (optical and microscopic analysis of particulate matter) of the soot formation process.[18] The lack of experimental data for intermediate-sized molecular species is due to the difficulty in identifying and quantifying species of this size, particularly in atmospheric, or higher pressure, flames.[18] As a consequence, considerable debate has occurred in the literature surrounding both the nature of the inception process and the identification of specific chemical species that may be involved in it.[19-21]

Our working hypothesis has been that inception begins with the agglomeration of PAH species that are large enough that "sticking" will occur at flame temperatures. In the mid-1980's Miller et al. used semi empirical atom pair potentials to estimate PAH intermolecular potentials.[22] From these potentials, second virial coefficients could be calculated leading to the equilibrium constants for dimerization reactions. The dimer concentrations calculated from these equilibria and the best available data for the concentrations of PAH monomers were significantly lower than the number densities of soot particles in flames[22]. Several years later, the problem was revisited from a kinetics perspective.[23] In this analysis, the dimer lifetimes were calculated assuming collision energy can either be accommodated by the agglomerate or be removed by collisions with molecules in the bath. Even though the collision accommodation model predicted faster forward rates for dimer formation, if equilibrium between dimers and monomers was assumed, dimer lifetimes did not change appreciably. To generalize, the results for both analyses indicated that agglomeration was only significant for collisions of PAH larger than 800 u (specifically for a reduced mass of the colliding pair of 400 u).[23] However, these results would have overestimated the size of monomer required for aggregation if the estimated concentrations of larger PAH ,which was inferred from the rapidly decreasing PAH size trends available at the time, were too low; if equilibrium did not exist between monomer and dimer concentrations; or if additional energy accommodation mechanisms were important.

Schuetz and Frenklach calculated dimer lifetimes of pyrene under flame conditions using a semi-empirical molecular dynamics approach.[24] They found that deposition of energy into internal rotations in the colliding pair greatly extended dimer lifetimes compared to the results we presented. Their predicted lifetimes grew rapidly with size, doubling between pyrene (202 u) and coronene (300 u) with a near linear trend. Schuetz and Frenklach suggested a lower size limit for PAH dimerization than we had originally proposed.[24] Subsequently, , many molecular growth numerical models consider species the size of pyrene as the transition between gas phase chemistry and particle growth dominated by aggregation.[25-30]

Results from recent soot formation models have concluded that pyrene dimers are not stable enough to aggregate at flame temperatures.[31-34] For example, Violi's group has used a combination of molecular dynamics simulations with the Metadynamics algorithm to study the free energy associated with dimerization of PAHs varying in molecular size and structure (ring types and presence/location of aliphatic linkages). While molecular geometry was found to play an important role in dimer stability, molecular size was the largest factor with the onset of dimerization possibly beginning with PAHs the size of ovalene (398 u).[34, 35] A similar size for the onset of aggregation was reported in a recent publication from the Kraft group at Cambridge who employed their population balance PAH-PP (polyaromatic hydrocarbon – primary particle) model[36, 37] coupled with KMC-ARS (kinetic Monte-Carlo-aromatic site). The collision efficiency for dimer formation was determined to be a function of the diameter and mass of the colliding PAH, where an efficiency of greater than 4% is necessary for substantial coagulation. These calculations showed that at flame temperatures particle inception with molecules as small as pyrene is unlikely, but could occur with a PAH in the 360-660 u range.[33]

The goal of the current contribution is to address the size of the agglomerating aromatics by interrogating young soot particles that form from them. Specifically we show that a hyper spectral measurement of extinction can be used to determine the particles' optical band gap, a quantity that correlates with the aromatic conjugation length. This work is complimentary to recent work in our laboratory in which conjugation length was determined by an analysis of collected nascent soot particles' Raman spectra.[21]

Extinction Measurements and Tauc Analysis

In the late 1960's, Tauc demonstrated that the low energy (long wavelength) edge of the optical absorption of amorphous semiconductors provides a probe of localized states.[38] Therefore the optical band gap (OBG), (for aromatic systems, presumably the energy difference between occupied and unoccupied π orbitals), can be calculated from **Equation 1.**

Eq 1.
$$h\upsilon \cdot \alpha \approx \left(h\upsilon - E_g^{opt}\right)^r$$

Where α is the extinction coefficient, E_g^{opt} is the OBG , and r is a constant that Tauc reports as usually being between 2 and 3.[38, 39] In 1970, Davis and Mott published a similar relationship, but questioned the validity of assumptions that Tauc made with respect to applications to the amorphous state. In their work, application to different materials and types of transitions lead to a wider range of values for r.[40] This lead to four common permutations describing the

directness and quantum mechanical allowedness of the optical transition: direct allowed (r = ½), direct forbidden (r = 3/2), indirect allowed (r = 2), and indirect forbidden (r = 3).[41]

The Tauc/Davis-Mott models suggest that the OBG may be experimentally determined from an extinction measurement. Building on Robertson's early theoretical work on the electronic structure of amorphous carbon,[42, 43] Robertson and Ferrari showed that systems with sp^2 character, such as soot, have electronic properties that are dominated by π-π* interactions. They then showed that the OBG scales inversely with the number of pericondensed aromatic rings in an aggregate (**Equation 2)**.

Eq 2.
$$E_g \approx \frac{2\gamma}{M^{\frac{1}{2}}} \approx 2\gamma\left(\frac{a}{L_a}\right)$$

where γ is a measure of ppπ interaction, M is the number of aromatic rings in a cluster, a is the lattice spacing, and L_a is the conjugation length.[44-46]

In the mid-1990's, D'Alessio [47-49] showed that absorption spectra collected at locations throughout sooting, premixed flames showed an evolution in OBG attributed to the chemical growth of soot precursors based on the relationship proposed by Robertson and Ferrari.[45, 46] Since this initial application of Tauc analysis to flame systems, this group and others have continued to utilize this method in a variety of laminar and turbulent premixed and non-premixed flames.[50-56]

Most recently, our group presented Tauc analysis for soot particulate in the inception region (2 cm above the burner surface) of a 60%-C_2H_4/40%-N_2 non premixed flame.[20] In this study, emission from a light emitting diode (LED), with its peak emission at 445 nm, was collimated, spatially filtered, and then focused in the flame. Transmitted light was recollimated and then directed into a spectroradiometer. After tomographic reconstruction of the radial extinction field, the OBG was derived using the Tauc analysis.[20] By averaging over all radial positions where substantial extinction was observed, an OBG of approximately 2.4 eV was reported.

In order to validate the relationship reported by Robertson and Ferrari (**Equation 2**), it was postulated that nascent soot particle morphology is dominated by clusters of moderately sized PAH and that the band gap of PAH in these structures could be estimated with the energy difference between the highest occupied and lowest unoccupied molecular orbitals in isolated PAH. The GAMESS-US computational chemistry package was used to perform time-dependent, density functional theory calculations, using the BLYP functional with the 6-31G* basis set, in order to calculate the electronic structure for several D_{2h} – symmetry PAH species, using optimized molecular geometries obtained from the *Theoretical Spectral Database Of Polycyclic Aromatic Hydrocarbons*.[57] The species studied were pyrene, ovalene, circumpyrene, and circumovalene, which span a range from 4 – 24 aromatic rings and 200 – 800 u. This range also covers the range discussed above in the context of PAH aggregation from pyrene [24-28] to larger molecular sizes.[7, 31, 33] By fitting these computational results to the relationship proposed by Robertson and Ferrari,[44-46] the following relationship (**Equation 3**) was observed, which correlates experimentally determined band gaps to the size of the PAH in the aggregate.

Eq 3.
$$E_g^{opt} = \frac{5.8076}{M^{1/2}} + 0.5413$$

Equation 2 also provides a relationship between the number of aromatic rings and the conjugation length. Given the carbon-carbon bond length in aromatic rings as 0.14 nm,[58] it is possible to use geometry to calculate the approximate area of a PAH in terms of its number of aromatic rings. Assuming PAH structure is dominated by pericondensed, nearly circular structures, the area of the PAH can also be used to estimate the diameter, which is a reasonable surrogate for the conjugation length. The approximation of conjugation length is beneficial in comparing our results to recent experimental and computational studies.[21, 33]

Using **Equation 3,** the measured band gap of 2.38±0.08 eV that we determined,[20] was correlated to a PAH with as few as 10 aromatic rings. In this initial analysis, the uncertainty was determined by averaging over different radial positions. Because the light source in this experiment was limited in spectral range and significantly bluer than the observed OBG, our experimental uncertainty may have been larger than what we reported due to the long extrapolation to the OBG.

In the current work, we are revisiting the extinction measurements utilizing Tauc/Davis-Mott analysis in a C_2H_4/N_2 flame system with four levels of dilution using a broadly tunable, supercontinuum light source. This source, with higher spectral range, substantially higher power, and spatial coherence, adds more fidelity to the prior measurements and its application to the complete set of flames allows for a more robust analysis of OBG.

Experimental

Burner and flame description

The burner used was designed and built at Yale University and has been extensively applied in flame structure studies by both our group and our collaborators at Yale using a variety of techniques.[20, 21, 59-66] Here, we report measurements in a series of atmospheric pressure, ethylene flames with the fuel diluted by nitrogen (from 32%-C_2H_4/68%-N_2 to 80%-C_2H_4/20%-N_2). The burner consists of a central fuel tube with an inner diameter of 0.4 cm and a concentric air co-flow tube with an inner diameter of 5.1 cm. The fuel flow at the nozzle exit has a parabolic profile with an average velocity of 35 cm/s with the air velocity profiles at the burner surface being plug flow of 35 cm/s. A stable flame is maintained using co-flowing air emitted from a honeycomb.[60] The burner is mounted on a motorized translational stage (Velmex BiSlide X15-Z10) that moves the burner both horizontally and vertically.

Extinction Measurements

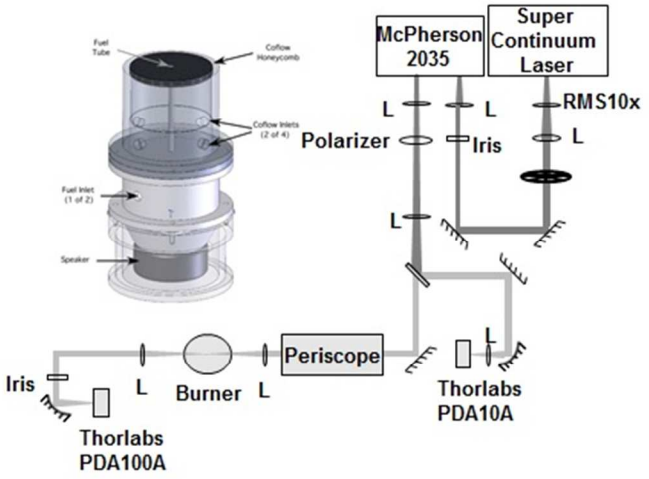

Figure 1: Experimental Schematic for line of sight extinction measurements (inset Burner schematic)

The experiment schematic is shown in ***Figure 1***. The light source used was a broadband super continuum light source (NKT Photonics EXB-4), which has spectral coverage from 425 nm to 2350 nm. The collimated beam from the laser was expanded from 0.11 cm to 1.1 cm, using a telescope system composed of an Olympus microscope objective (Thorlabs RMS10x) and a 100 mm focal length (*f.l.*) achromat (ThorLabs AC254-100A) mounted in a Thorlabs cage system. The beam was then directed through a chopper (Stanford Research Systems SR540) before being redirected by a pair of kinematically mounted flat mirrors. The reorientation of the beam allowed for it to be focused onto the entrance slit of a monochromator using a 50 mm *f.l.* achromat (Thorlabs AC254-50-A), where an iris was used to block stray light. A McPherson Model 2035 monochromator with a 1200 grooves/mm grating blazed at 500 nm was used. Using a 1.25 mm slit width the system provided approximately 2 nm resolution over the experimental spectral range. The beam passed through the monochromator, to another 50 mm *f.l.* achromat to recollimate, a polarizer (Thorlabs LPVISE200-A) in a rotational mount, and a 200 mm *f.l.* achromat (AC254-200-A) which directed the beam onto a beam splitter (ThorLabs CM1-BS013). The beam splitter divided the experiment into two channels, one that was directed through the flame and one that bypassed the flame, generating a channel for the extinction measurements and a channel for measuring power fluctuations. The power-monitoring channel was comprised of a flat mirror, a parabolic mirror (ThorLabs MPD254508-90-P01), a 50 mm *f.l.* achromat (ThorLabs AC254-50-A), and a diffuser (Thorlabs DG10-600-MD), which all function to focus the beam onto the surface of a photodiode detector (ThorLabs PDA10A). The transmitted light channel was periscoped into the flame using a set of flat mirrors and then focused into the center of the flame using a 100 mm *f.l.* achromat (ThorLabs AC254-100-A). At the focal point, the beam waist is 0.47 mm in the horizontal direction. Downstream of the flame, the beam was collimated by a 100 mm *f.l.* achromat (ThorLabs AC254-100-A). The beam was then redirected by a flat mirror through an iris to a parabolic mirror (ThorLabs MPD254508-90-P01). The iris was used to minimize the effect of flame radiation in the extinction measurement. The beam was then focused onto a second photodiode detector (ThorLabs PDA100A), which also had a mounted diffuser (Thorlabs DG10-600-MD) facilitating detection. A pair of lock-in amplifiers (Stanford Research Systems SRS810 and Stanford Research Systems SRS 850) were connected to the two detection channels and connected to a computer. The chopper, at 400 Hz, was used as the external reference for both lock-in amplifiers.

The Enthought Canopy python environment suite was used to develop a program that combines control of the monochromator, translational stage, and lock-in amplifiers to automate the data collection procedure. By initially defining the experimental parameters, the program moved to the defined start height above the burner (HAB), lateral position, and wavelength. The program conducted scans over the entire horizontal position range, -1.0 cm to 1.0 cm in 0.05 cm increments, at each wavelength. After completing the scan, the positioner would return to the starting position and the monochromator would move 2 nm to the next wavelength. The procedure was repeated until the entire spectral range, 440 nm to 540 nm, was covered. The program was then run at the range of HABs from 0.5 cm height above burner (HAB) to the where extinction was no longer observed, in 0.5 cm increments.

Data Analysis

In the reported extinction data line of sight projection measurements are made in axi-symmetric flame, from 1.0 cm on either side of the flame center in 0.05 cm increments. Because of the complex power structure of the light source, the laser intensity at the sampled regions outside of the flames is used as the baseline in calculating the extinction. The power metering channel is used to ensure that there is no significant deviation in the laser power over a position scan.

Because the flame is axi-symmetric, the raw extinction will be a combination of contributions from the different radial positions the laser beam passes through. In a line of sight measurement the beam direction is labelled as X and the sampling direction is Y. The line of sight extinction signal P(y, λ) at a given wavelength collected across the axi-symmetric flame can be related to radial extinction, f(r,λ) (**Equation 4**).

$$P(y,\lambda) = ln\left(\frac{I}{I_o}\right)_{y,\lambda} = 2\int_0^x f(r,\lambda)dx$$

Eq 4.

In order to recover the radially-distributed data, a 3 point Abel inversion is performed, using an approach adapted from Dasch.[67] In the past our group has used this tomographic reconstruction approach for tunable diode laser absorption spectroscopy [68] and in the Tauc extinction measurements using an LED.[20] The deconvolved extinction signal, $F(r_i, \lambda)$, is calculated from the line of sight data through **Equation 5.**

$$F(r_i,\lambda) = \frac{1}{\Delta r}\sum_{\infty}^{j=0} D_{ij}P(y_j,\lambda)$$

Eq 5.

In this relationship Δr is the spacing in the line of sight measurements, 0.05 cm, the subscripts i and j are indices of the

radial and line of sight coordinates, and D_{ij} is a matrix of coefficients determined by Dasch for a 3-point Abel inversion.

The Abel inversion procedure typically degrades the signal to noise ratio of the measurements, making it necessary to input smoothed, symmetric, and centered line of sight profiles to minimize these effects. In this work, intensity as a function of wavelength at each position is smoothed by fitting to an exponential function prior to the tomographic reconstruction. In this fit (**Equation 6**), α is extinction, a,b,c are fitting parameters, and λ is wavelength.

Eq 6. $$\alpha = ae^{-b\lambda} + c$$

By fitting the spectral data prior to the Abel inversion, it is possible to quantify how noisy the data is in relation to the fit (ratio of residual sum of squares to total sum of squares), and therefore error propagation can be used to see how this noise translates to uncertainty in the determination of the OBG. Because this method only accounts for uncertainty caused from the fitting procedure onward, it is necessary to consider the error caused by the calculation of the extinction using baseline fits separately. **Figure 2** depicts a line of sight extinction spectra taken over two experimental sessions, leading to a slight discontinuity in the two data sets. To quantify the uncertainty in the calculation of the extinction and day-to-day variability in the system the standard deviation in OBG at each radial position in replicate HAB 2 cm experiments was taken. The reported error in the OBG is the sum of the uncertainty caused from calculating the extinction and the error propagated exponential fit.

Results and Discussion

Figure 2 shows the resulting line of sight extinction in the 60%-C_2H_4/40%-N_2 flame 0.2 cm from the centerline and 2.0 cm above the burner. In this figure the symbols represent the experimental data, where the dashed line is the data modelled with the exponential fit (**Equation 6).** ***Figure 3*** illustrates the data collected in the 60%-C_2H_4/40%-N_2 flame 2.0 cm above the burner at 500 nm, where the squares are the experimental data and the solid line is the model generated by the spectral fit

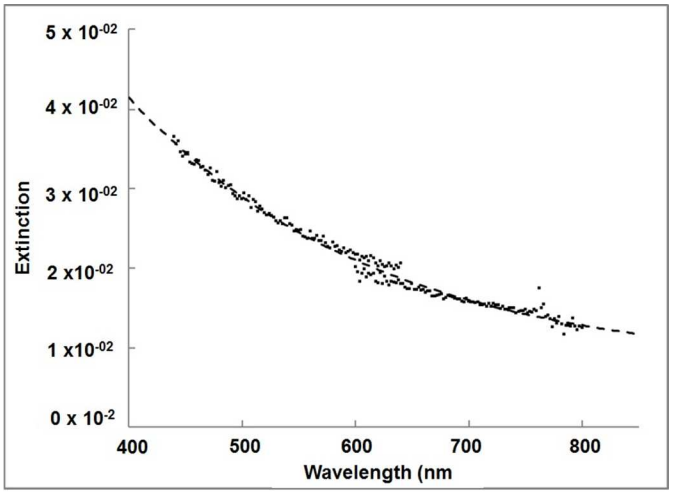

Figure 2: Symbols: Line of sight extinction spectra collected 2 cm above the burner 0.20 cm from the centerline of the flame over two experimental sessions. Dashed Line: Exponential fit of line of sight extinction data. The noise of the experimental data compared to the fit is 2.65%. Taking data over two sessions leads to the discontinuity seen in the figure, which is accounted for in the error analysis protocol.

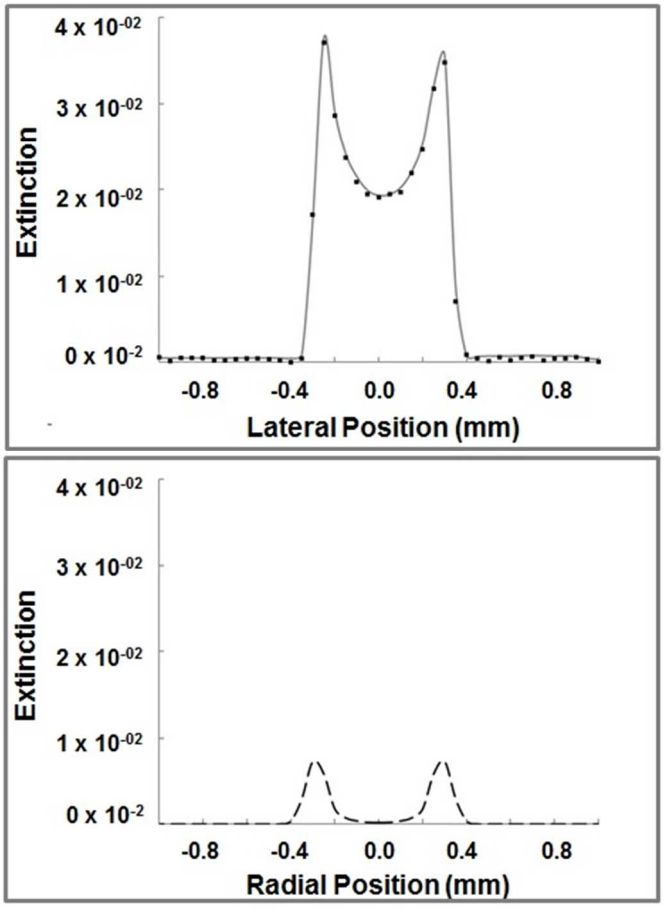

Figure 3: Top Chart: Line of sight extinction data at 500 nm for data collected 2 cm above the burner (squares – experimental data and solid line – result from the exponential fit). Bottom Chart: Radially distributed extinction data (dashed line) from tomographic reconstruction at 500 nm for data collected 2 cm above the burner.

Soot Volume Fraction (SVF)

In a recent publication of from our lab and our collaborators at Yale, Raman and Laser Induced Incandescence (LII) measurements were correlated with a direct numerical simulation of molecular growth chemistry.[21] In this work the LII experiments were calibrated via an extinction measurement based on the following relationship (Equation 7).[69]

Eq 7. $$f_v = \frac{-ln(\frac{I}{I_0})\lambda}{lK_e}$$

where f_v is the soot volume fraction, I/I_0 is the ratio transmitted to incident light, l is the path length, λ is the wavelength of light, and K_e is the dimensionless extinction coefficient of soot taken to be 8.6 within laminar diffusion flames.[70, 71] In this flame system, scattering has been historically ignored[60] because of the modest soot volume

fraction compared to other flame systems.[72] By taking $-ln(I/I_0)$ to be our radially distributed extinction and l to be the tomographic reconstruction step of 0.05 cm, we were able to calculate the soot volume fraction for the entire flame system and compare it to computed soot volume fraction from the direct numerical simulation of molecular growth chemistry data from the Smooke Group at Yale and Laser Induced Incandescence (LII) data from the Long Group at Yale (60%-C_2H_4/40%-N_2 Flame shown in Figure 4 with other dilutions shown in Supplementary Data).[21, 60] In both sets of experimental data and the computations, the general shape of the soot field is similar with the experimental data appearing sharper at the flame tip than the computations. In all data sets the first observable particle concentrations are between 0.5 cm and 1.0 cm above the burner's surface and it is also possible to observe the migration of maximum soot concentrations from the center of the flame in the low sooting flames to the wings in the higher sooting flames. Our experimental soot volume fractions have lower spatial resolution than the calculations, causing the annular regions to be somewhat spatially degraded with the effect becoming more pronounced with increasing nitrogen dilution. In both SVF calculated from our extinction measurements and SVF from LII, the reported SVF are higher than those computed by the Yale model. While all three data sets use the same dimensionless extinction coefficient, the uncertainty in this value and its effect on the calculation of SVF is worthy of discussion.

Williams et al. report values of K_e for a range of fuels and at two wavelengths using extractive sampling.[71] While they report values that are consistent with prior literature, they also discuss the dependence on both wavelength and fractal morphology which may be variable in different flame systems.[71] In a laminar, pure ethylene flame the soot particles begin as isolated primary particles for which scattering is minimal to large fractal aggregates where scattering accounts for up to 20% of extinction.[71] This almost certainly would cause changes in the cross sections and refractive indices observed throughout the flame. While Williams et al. did not observe a systematic change in K_e throughout their ethylene flame; their reported values span a range of K_e values in the ethylene flame from 8 to 10. Using these values to calculate the soot volume fraction changes the result by over 20%, in addition to an up to 5% change that is caused by using the same K_e value over the relatively short 100 nm spectral range.

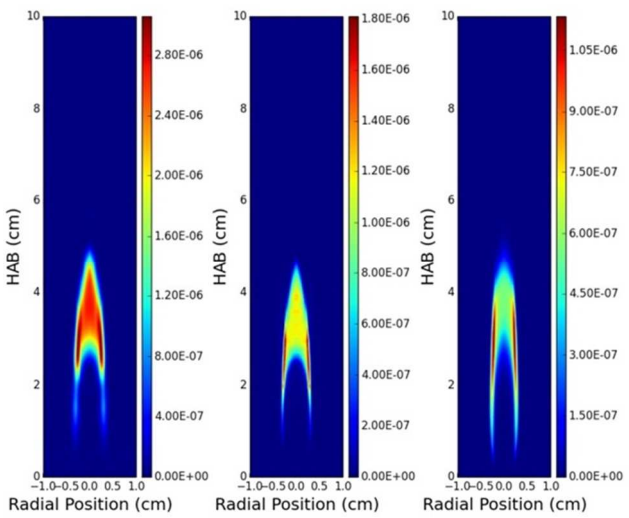

Figure 4: Left: Calculated SVF from line of sight Extinction data at 500nm. Middle: LII data from Long group at Yale. Right: Computed SVF from Smooke group at Yale. All data sets shown are for the 60%-C_2H_4/40%-N_2 flame. Figures for other dilution levels are available in the supplementary materials.

OBG Calculation

As noted in the introduction the Tauc/Davis-Mott analysis method requires an assumption about the type of band gap and quantum mechanical allowedness of the transition being studied. Starting with the work by D'Alessio the application of Tauc analysis to combustion systems has almost universally assumed an *r* value of 2, which corresponds to an allowed indirect band gap.[47-49, 73] Our assumption is that soot particles are comprised of condensed aromatic systems of high symmetry and it is reasonable to assume that the transitions are quantum mechanically allowed. However, is the transition direct or indirect?. Seo and Hoffmann describe the complicated nature of predicting the type of band gap transition in stacked conjugated systems based on the overlapping carbon sites. In a study of naphthalene, they show that band gap type is determined by the stacking arrangement. In this case perfectly overlapped stacks (known as "eclipsed" in much of the PAH intermolecular potential literature) result in indirect optical band gaps, where the slipped configuration can give rise to either a direct or indirect band gap based on the interacting carbon sites.[74] Recent calculations for structures of larger PAH stacks also suggest that the eclipsed geometry is less favourable than slipped structures.[75, 76]

The Davis-Mott literature also suggests that in addition to prior knowledge (or even intuition) the results of testing different values of *r* in the Tauc/Davis-Mott can provide insight.[40, 41, 77] In this data set, the tomographically reconstructed data was plotted by a manipulated **Equation 1**, where $(\alpha \cdot h\nu)^{1/r}$ was plotted as a function of photon energy (eV), converted from wavelength. The use of $r = 0.5$, corresponding to an allowed, direct band gap, resulted in the typical Tauc/Davis-Mott plot with a straight line portion at high photon energies and moving into a curved portion as the Urbach region was reached at lower photon energies. OBGs were calculated by extrapolating the straight line portion plot to the x-intercept.

A challenge in the application of the Tauc/Davis-Mott model is presented by the gradual transition from the straight line portion into the curved Urbach region. If this portion of the extinction curve is included, the OBG will be lowered. The cause of the Urbach region has no single explanation, having been attributed to transitions between localized states, bound exciton interaction with lattice vibrations, electric field broadening of the absorption edge, and electric field broadening of an exciton line.[38, 40, 41, 77] In any case, the selection of the spectral range used in the Tauc/Davis-Mott analysis is important because the interpolated OBG will be highly dependent on this selection. To determine the spectral range to be used in the fit of OBG, several spectral were collected for an extended range of wavelengths: (440 nm to 800 nm) at 2.0 cm above the burner in the 60%-C_2H_4/40%-N_2 flame (**Figure 2)** and the tomographically reconstructed data were plotted **(Figure 5).** Lines of best fit were drawn through the data as the long wavelength limit was varied. Sensitivity of linearity to this low energy limit were most noticeable in the center of the flame, where there is lower soot concentration, For all locations the linearity started to decrease more for spectral endpoints greater than 540 nm Therefore, the spectral range of 440 nm to 540 nm was used for all subsequent analysis. Additionally, only fits for which R^2 exceeded 0.9 are reported in subsequent analysis.

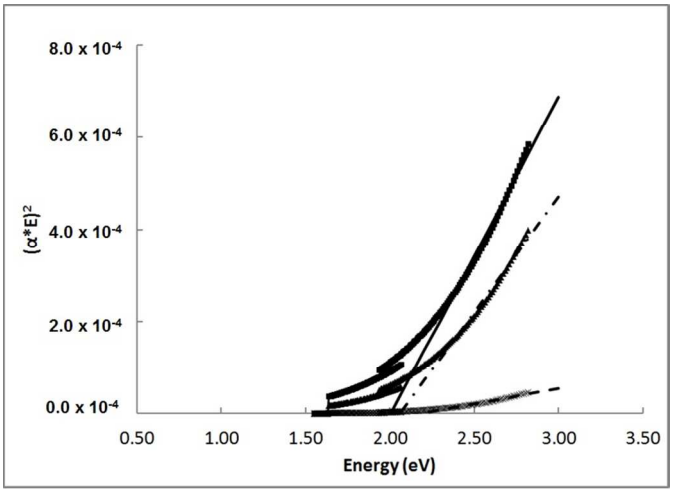

Figure 45: Tauc analysis plot for radially-resolved extinction HAB2cm for 0.20 cm (data – X, fit – dashed line), 0.25 cm (data – triangle, fit – dash dot line), and 0.30 cm (data – square, fit – solid line) from the burner centerline. The optical band gaps calculated from three linear fits are 2.14 eV ± 0.05 (0.20 cm), 2.07 eV ± 0.04 (0.25cm), and 2.04 eV ± 0.04 (0.30cm).

This approach was repeated at radial positions where there was substantial soot concentrations present at each HAB, for all of the flame systems. For consistency, substantial soot concentration was defined as a soot volume fraction, computed by direct numerical simulation of molecular growth chemistry by our collaborators at Yale,[21, 60] of greater than 0.01 ppm. **Figure 6** depicts the experimentally determined OBG including propagated error at 2.0 cm above the burner in the 60%-C_2H_4/40%-N_2 flame. This figure also depicts the computed soot volume fraction for reference. There is a clear evolution in the OBG as a function of radial position where the OBG is lowest in the region where the soot volume fraction is the highest.

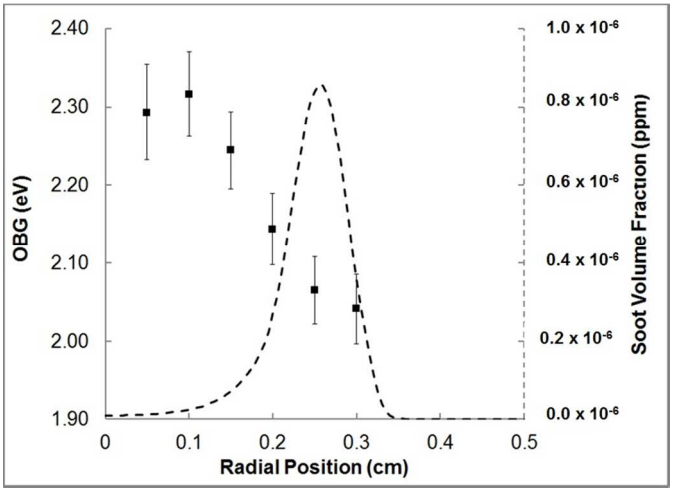

Figure 56: Experimentally determined OBG (squares) as a function of radial position at 2.0cm above the burner (60%-C_2H_4/40%-N_2).

The solid line depicts the soot volume flame calculated by the Smooke Group at Yale at the same flame position.

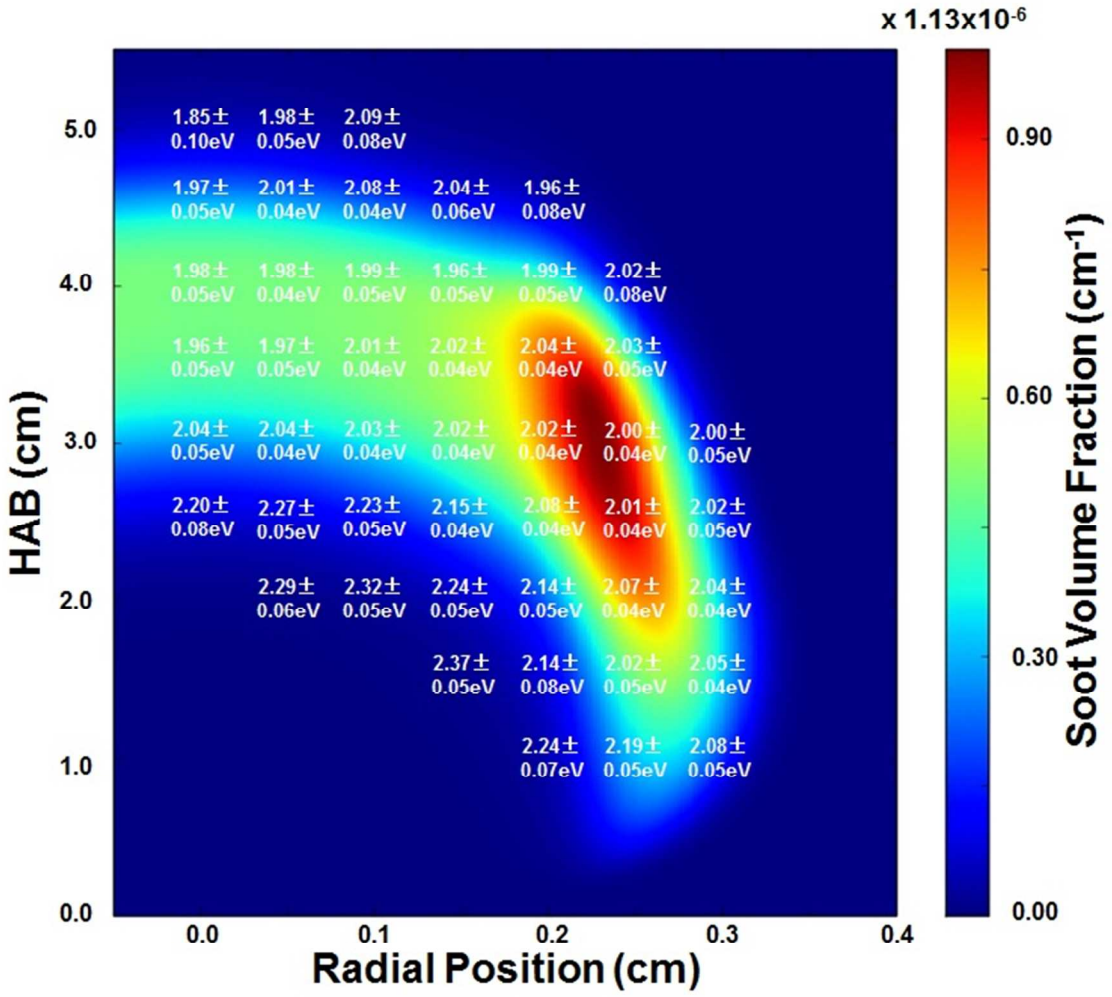

Figure 6~~7~~: Experimentally determined OBG overlaid on contour plots of soot volume fraction calculated by the Smooke group at Yale for the 60%-C_2H_4/40%-N_2 flame

Figure 7 depicts computed soot volume fraction as a function of flame position with the experimentally determined OBG overlaid for the 60%-C_2H_4/40%-N_2 system. The amount of data and fidelity of the data increases as we move to the heavier sooting flames. The consistency of the OBG calculated over the flame systems supports the validity in ignoring scattering during Tauc/Davis-Mott analysis. Correlating with an analysis of the soot formation submodels reported by Smooke et al., the OBG decreases through the inception and surface growth regions and there is a slight increase in the OBG in the oxidation regions of the flame.[60] Using the relationship proposed by Robertson and Ferrari (**Equation 2**), this means that PAHs making up the soot particles tend to be slightly larger in the areas where the soot volume fraction is larger.

Correlation to Molecular Size

As described in the introduction, **Equation 3** was used to correlate the experimentally determined OBG to PAH size.[20] ***Figure 8*** combines the relationship between the number of aromatic rings and the OBG and the relationship between the number of aromatic rings and the conjugation length to relate the experimentally determined OBG to the physical size of the PAH it belongs to for the 60%-C_2H_4/40%-N_2 flame. The grey bands represent how the range of experimentally determined OBG throughout each flame correlate with the number of aromatic rings and number of aromatic rings correlate with conjugation length. If the magnitude of soot volume fraction depended only on chemical growth, the longer residence times in the 60% and 80% flames would be expected to produce larger PAH and smaller OBG. Instead we observe nearly the same OBG (and thus size of PAH, 10-20 rings) for all flames. The average OBG of 2.09 eV corresponds to a PAH with 14 aromatic rings and a conjugation length of about 0.97 eV; a molecule about the size of circumpyrene.

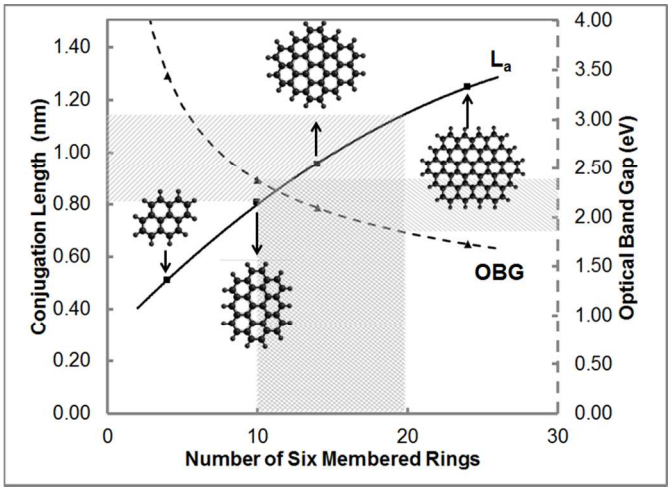

Figure 7~~8~~: Comparison between calculated HOMO-LUMO energy gaps (OBG) with number of aromatic rings and conjugation length. The dashed line and triangle show the relationship between OBG and number of rings. The solid line and squares show the relationship between conjugation length and number of rings. The grey bands depict how the range of OBG observed throughout the 60%-C_2H_4/40%-N_2 flame correlate to physical morphology parameters.

The OBG values reported here differ substantially from those reported in the work by D'Alessio et al and subsequent work from collaborating groups.[47-49, 51, 52, 54-56] The difference in our results may be attributed to the choice of r value assumed in Equation 1, our different approaches to fitting the Urbach region, and the possibility that soot may have a different morphology in different flame systems. Interestingly, a recent publication from the Russo group reports fringe length measurements from high resolution electron transmission microscopy studies that range from 0.94 nm to 1.24 nm and conjugation lengths from Raman studies from 1.03 nm to 1.13 nm in an ethylene flame[78] in agreement with the range of conjugation lengths determined in this study. Their publication also correlates the measured fringe lengths to the number of aromatic rings, finding the most common probable structure containing a 4 by 4 ring structure, which is similar to the size of circumpyrene.[78]

The current results correspond well with experimental and computational results from our lab and the Kraft group at Cambridge. In recent studies from our lab, we analyzed Raman scattering signals in the inception region of the flame and found that the source of scattering was a PAH species with a conjugation length of 1.0-1.2 nm[21]. The computational work done by the Kraft group reported particle inception beginning with PAH with conjugation lengths about 1.0 nm and 360 u.[33] .

The size suggested for aggregation is likely more qualitative than quantitative. The extinction behaviour for nascent soot particles is more complicated than the extinction of the PAH that agglomerate to form the particle. For example, as our calculations [79] (and those of others) have shown, aggregation of aromatics increases the density of states near the HOMO-LUMO gap which might be revealed as a lowering in the band gap. Further, as noted above, the result of the Tauc/Davis-Mott analysis depends on the selection of spectral range, but it also may be more heavily influenced by the larger PAHs in the aggregate.

Conclusions

Light from a supercontinuum light source was used to measure light extinction in a series of nitrogen diluted ethylene, non-premixed flames. The tomographically reconstructed extinction data was processed using Tauc/Davis-Mott analysis to determine the optical band gap. The average OBG at all positions was 2.09 ± 0.10 eV showing a range of results from about 1.85 eV to 2.35 eV. This result was then compared to previously published computational results from our lab relating calculated HOMO-LUMO gaps for a series of D_{2h} molecules to the number of aromatic rings in the structure[20]. From this relationship, the measured OBG suggests an average PAH size of about 14 rings and a range of 10-20 rings throughout the flames. A conjugation length of ≈ 0.97 nm corresponds to a PAH of this average size. This result is consistent with the lower size bound for aromatic structures determined from Raman spectra of thermophertically-sampled carbonaceous material in the same flames systems. The median conjugation length matches with the critical PAH size for particle inception reported in recent computational studies.[21, 33]

Acknowledgements

This material is based upon work supported by the U.S. National Science Foundation under grants CBET-0828950 and CBET-1142284 with Drs. Philip Westmoreland, Avind Atreya, and Ruey-Hung Chen serving as technical monitors. We would like to thank our colleagues, Marshall Long and Mitchell Smooke and their research groups, at Yale University for a continuous, productive collaboration.

Notes and references

[a] Department of Chemistry, George Washington University, 725 21st St., NW, Room 107, Washington, DC 20052, USA

Electronic Supplementary Information (ESI) available: Plots of Experimentally determined OBG overlaid on contour plots of soot volume fraction calculated by the Smooke group at Yale for the entire flame system and comparison between calculated HOMO-LUMO energy gaps (OBG) with number of aromatic rings and conjugation length for the entire flame system. See DOI: 10.1039/b000000x/

1. U. S. E. I. Administration, *Annual Energy Outlook 2014 with projections to 2014*, 2014.
2. E. Sasser, J. Hemby, K. Adler, S. Anenberg, C. Bailey, L. Brockman, L. Chappell, B. J. DeAngelo, R. Damberg, J. Dawson, N. Frank, M. Geller, G. Hagler, B. Hemming, L. Jantarasami, T. Luben, J. Mitchell, J. Moss, V. Rao, J. Rice, M. C. Sarofim, J. Sommers, C. Spells, S. Terry and M. Witosky, *Report to Congress on Black Carbon*, Department of the Interior, Environment, and Related Agencies, 2012.
3. T. C. Bond, S. J. Doherty, D. W. Fahey, P. M. Forster, T. Berntsen, B. J. DeAngelo, M. G. Flanner, S. Ghan, B. Kärcher, D. Koch, S. Kinne, Y. Kondo, P. K. Quinn, M. C. Sarofim, M. G. Schultz, M. Schulz, C. Venkataraman, H. Zhang, S. Zhang, N. Bellouin, S. K. Guttikunda, P. K. Hopke, M. Z. Jacobson, J. W. Kaiser, Z. Klimont, U. Lohmann, J. P. Schwarz, D. Shindell, T.

Storelvmo, S. G. Warren and C. S. Zender, *Journal of Geophysical Research: Atmospheres*, 2013, **118**, 5380-5552.
4. J. H. Butler, S. A. Montzka, E. J. Dlugokencky, J. W. Elkins, K. A. Masari, R. C. Schnell and P. P. Tans, EGU General Assembly Conference Abstracts, 2013.
5. M. E. G.-N. Nicole AH Janssen, Timo Lanki,, F. C. Raimo O Salonen, Gerard Hoek, and B. B. Paul Fischer, Michal Krzyzanowski, *Health Effects of Black Carbon*, 2012.
6. M. Frenklach and L. B. Ebert, *The Journal of Physical Chemistry*, 1988, **92**, 561-563.
7. H. Wang and M. Frenklach, Fall Technical Meeting of the Eastern States Section of the Combustion Institute, Albany, New York, Paper, 1989.
8. M. Frenklach and H. Wang, *Proceedings of the Combustion Institute*, 1991, **23**, 1559-1566.
9. H. Wang and M. Frenklach, *The Journal of Physical Chemistry*, 1993, **97**, 3867-3874.
10. H. Wang and M. Frenklach, *Combustion and flame*, 1997, **110**, 173-221.
11. M. Frenklach and H. Wang, *Proceedings of the Combustion Institite*, 1998, **23**, 1559-1566.
12. M. Frenklach, *Physical Chemistry Chemical Physics*, 2002, **4**, 2028-2037.
13. N. Moriarty, X. Krokidis, W. Lester Jr and M. Frenklache, ABSTRACTS OF PAPERS OF THE AMERICAN CHEMICAL SOCIETY, 2002.
14. M. Frenklach and H. Wang, *Symposium (International) on Combustion, [Proceedings]*, 1991, **23rd**, 1559-1566.
15. K.O. Johansson, S. A. S. J.Y.W. Lai, D.M. Popolan-Vaida, N. H. K.R. Wilson and H. A. M. A. Violi, *Proceedings of the Combustion Institite*, 2014, **35**.
16. S.-H. Chung and A. Violi, *Proceedings of the Combustion Institute*, 2011, **33**, 693-700.
17. H. Richter and J. Howard, *Progress in Energy and Combustion Science*, 2000, **26**, 565-608.
18. P. Desgroux, X. Mercier and K. A. Thomson, *Proceedings of the Combustion Institute*, 2013, **34**, 1713-1738.
19. J. Happold, H.-H. Grotheer and M. Aigner, *Rapid Communications in Mass Spectrometry*, 2007, **21**, 1247-1254.
20. J. H. Miller, J. D. Herdman, C. D. O. Green and E. M. Webster, *Proceedings of the Combustion Institute*, 2013, **34**, 3669-3675.
21. J. D. Herdman, B. C. Connelly, M. D. Smooke, M. B. Long and J. H. Miller, *Carbon*, 2011, **49**, 5298-5311.
22. J. H. Miller, W. G. Mallard and K. C. Smyth, *The Journal of Physical Chemistry*, 1984, **88**, 4963-4970.
23. J. H. Miller, *Proceedings of the Combustion Institute*, 1991, **23**, 91-98.
24. C. A. Schuetz and M. Frenklach, *Proceedings of the Combustion Institute*, 2002, **29**, 2307–2314.
25. J. Z. Wen, M. Thomson, S. Park, S. Rogak and M. Lightstone, *Proceedings of the Combustion Institute*, 2005, **30**, 1477-1484.
26. J. Singh, R. I. Patterson, M. Kraft and H. Wang, *Combustion and Flame*, 2006, **145**, 117-127.
27. S. B. Dworkin, Q. Zhang, M. J. Thomson, N. A. Slavinskaya and U. Riedel, *Combustion and Flame*, 2011, **158**, 1682-1695.
28. J. Appel, H. Bockhorn and M. Frenklach, *Combustion and Flame*, 2000, **121**, 122-136.
29. A. Kazakov, H. Wang and M. Frenklach, *Combustion and Flame*, 1995, **100**, 111-120.
30. X.-S. Bai, M. Balthasar, F. Mauss and L. Fuchs, *Proceedings of the Combustion Institute*, 1998, **27**, 1623-1630.
31. H. Wang, *Proceedings of the Combustion Institute*, 2011, **33**, 41-67.
32. H. Sabbah, L. Biennier, S. J. Klippenstein, I. R. Sims and B. R. Rowe, *The Journal of Physical Chemistry Letters*, 2010, **1**, 2962-2967.
33. E. K. Yapp and M. Kraft, in *Cleaner Combustion*, Springer, 2013, pp. 389-407.
34. P. Elvati and A. Violi, *Proceedings of the Combustion Institute*, 2013, **34**, 1837-1843.
35. J. S. Lowe, J. Y. Lai, P. Elvati and A. Violi, *Proceedings of the Combustion Institute*, 2014.
36. M. Sander, R. I. A. Patterson, A. Braumann, A. Raj and M. Kraft, *Proceedings of the Combustion Institute*, 2011, **33**, 675-683.
37. D. Chen, Z. Zainuddin, E. Yapp, J. Akroyd, S. Mosbach and M. Kraft, *Proceedings of the Combustion Institute*, 2013, **34**, 1827-1835.
38. J. Tauc, R. Grigorovici and A. Vancu, *physica status solidi (b)*, 1966, **15**, 627-637.
39. D. L. Wood and J. Tauc, *Physical Review B: Solid State*, 1972, **[3]5**, 3144-3151.
40. E. Davis and N. Mott, *Philosophical Magazine*, 1970, **22**, 0903-0922.
41. E. A. Davis and N. F. Mott, *Electronic Processes in Non-Crystalline Materials*, 2 edn., Oxford University Press, Oxford, 2012.
42. J. Robertson and E. P. O'Reilly, *Physical Review B: Condensed Matter and Materials Physics*, 1987, **35**, 2946-2957.
43. J. Robertson, *World of Carbon*, 2001, **1**, 249-273.
44. L. G. Cancado, K. Takai, T. Enoki, M. Endo, Y. A. Kim, H. Mizusaki, A. Jorio, L. N. Coelho, R. Magalhaes-Paniago and M. A. Pimenta, *Applied Physics Letters*, 2006, **88**, 163106-163101-163106-163103.
45. A. C. Ferrari and J. Robertson, *Physical Review B: Condensed Matter and Materials Physics*, 2000, **61**, 14095-14107.
46. A. C. Ferrari and J. Robertson, *Physical Review B*, 2001, **64**, 075414-075411-075414-075413.
47. P. Minutolo, G. Gambi and A. D'Alessio, *Proceedings of the Combustion Institute*, 1996, **26th**, 951-957.
48. A. D'Alessio, A. D'Anna, G. Gambi and P. Minutolo, *Journal of Aerosol Science*, 1998, **29**, 397-409.
49. A. D'alessio, G. Gambi, P. Minutolo, S. Russo and A. D'Anna, *Symposium (International) on Combustion*, 1994, **25**, 645-651.
50. G. Basile, A. Rolando, A. D'Alessio, A. D'Anna and P. Minutolo, *Proceedings of the Combustion Institute*, 2002, **29**, 2391-2397.
51. C. Allouis, A. D'Alessio, F. Beretta and A. Borghese, *Proceedings of the Combustion Institute*, 2000, **28**, 311-317.
52. A. Ciajolo, B. Apicella, R. Barbella and A. Tregrossi, *Combustion Science and Technology*, 2000, **153**, 19-32.
53. B. Apicella, M. Alfè, R. Barbella, A. Tregrossi and A. Ciajolo, *Carbon*, 2004, **42**, 1583-1589.
54. C. Russo, M. Alfè, J.-N. Rouzaud, F. Stanzione, A. Tregrossi and A. Ciajolo, *Proceedings of the Combustion Institute*, 2013, **34**, 1885-1892.
55. C. Russo, F. Stanzione, A. Ciajolo and A. Tregrossi, *Proceedings of the Combustion Institute*, 2013, **34**, 3661-3668.
56. C. Russo, F. Stanzione, M. Alfè, A. Ciajolo and A. Tregrossi, *Combustion Science and Technology*, 2012, **184**, 1219-1231.
57. G. Malloci, 2011, vol. 2011.
58. R. T. Sanderson, *Science*, 1952, **116**, 41-42.
59. M. D. Smooke, R. J. Hall, M. B. Colket, J. Fielding, M. B. Long, C. S. McEnally and L. D. Pfefferle, *Combustion Theory and Modelling*, 2004, **8**, 593-606.
60. M. D. Smooke, M. B. Long, B. C. Connelly, M. B. Colket and R. J. Hall, *Combustion and Flame*, 2005, **143**, 613-628.
61. S. A. K. Blair C Connelly, Mitchell D Smooke, Marshall B Long, *Proceedings of the US Sections of the Combustion Institute*, 2005, **4**.
62. S. B. Dworkin, M. D. Smooke and V. Giovangigli, *Proceedings of the Combustion Institute*, 2009, **32**, 1165-1172.
63. M. A. Puccio, J. D. Herdman, J. H. Miller, B. C. Connelly, M. D. Smooke and M. B. Long, *Chemical and Physical Processes in Combustion*, 2005, 217-220.
64. B. C. Connelly, B. A. Bennett, S. Dworkin, M. D. Smooke, M. B. Long, M. A. Puccio, J. D. Herdman and J. H. Miller, *Chemical and Physical Processes in Combustion*, 2005, 259-262.
65. S. B. Dworkin, B. C. Connelly, A. M. Schaffer, B. A. V. Bennett, M. B. Long, M. D. Smooke, M. P. Puccio, B. McAndrews and J. H. Miller, *Proceedings of the Combustion Institute*, 2007, **31**, 971-978.
66. B. M. M. B. Long, 8th US Combustion Institute, 2013.
67. C. J. Dasch, *Appl. Opt.*, 1992, **31**, 1146-1152.
68. R. R. Skaggs and J. H. Miller, *Combustion anf Flame*, 1995, **100**, 430-439.

69. H. Zhao and N. Ladommatos, *Progress in Energy and Combustion Science*, 1998, **24**, 221-255.
70. S. Krishnan, K.-C. Lin and G. Faeth, *Journal of Heat Transfer*, 2001, **123**, 331-339.
71. T. C. Williams, C. Shaddix, K. Jensen and J. Suo-Anttila, *International Journal of Heat and Mass Transfer*, 2007, **50**, 1616-1630.
72. R. Santoro, H. Semerjian and R. Dobbins, *Combustion and Flame*, 1983, **51**, 203-218.
73. P. Minutolo, G. Gambi and A. D'Alessio, *Proceedings of the Combustion Institute*, 1996, **26**, 951-957.
74. D.-K. Seo and R. Hoffmann, *Theoretical Chemistry Accounts*, 1999, **102**, 23-32.
75. J. D. Herdman and J. H. Miller, *Journal of Physical Chemistry A*, 2008, **112**, 6249-6256.
76. S. Grimme, *Journal of computational chemistry*, 2004, **25**, 1463-1473.
77. X. Li, H. Zhu, J. Wei, K. Wang, E. Xu, Z. Li and D. Wu, *Applied Physics A*, 2009, **97**, 341-344.
78. B. Apicella, P. Pré, M. Alfè, A. Ciajolo, V. Gargiulo, C. Russo, A. Tregrossi, D. Deldique and J. N. Rouzaud, *Proceedings of the Combustion Institute*.
79. J. H. Miller, *Proceedings of the Combustion Institute*, 2005, **30**, 1381-1388.